Progress In Electromagnetics Research C, Vol. 27, 129–142, 2012

MULTILAYER DIELECTRIC RESONATOR ANTENNA TRANSMITARRAY FOR NEAR-FIELD AND FAR-FIELD FIXED RFID READER

S. H. Zainud-Deen[1], S. M. Gaber[2], H. A. Malhat[1,*], and K. H. Awadalla[1]

[1]Faculty of Electronic Engineering, Menoufia University, Egypt

[2]Cairo Higher Institute of Engineering, Cairo, Egypt

Abstract—A design of multilayer dielectric resonator antenna transmitarray for fixed radio frequency identification (RFID) reader applications is presented at 5.8 GHz. Three layers square dielectric resonator antenna (DRA) elements are mounted on dielectric substrate and used as a unit cell in the transmitarray. A circularly polarized 9×9 square DRA transmitarray is designed at 5.8 GHz for far-field RFID applications. The transmitarray produces maximum gain of 20.2 dB. The right-hand circular polarization level is lower than -31 dB at the designed frequency with SLL of -22 dB. A design of 9×9 near-field focused DRA transmitarray for fixed RFID at 5.8 GHz is investigated. The properties of the near field-focused transmitarray are compared with that of the far field transmitarray designed at the same operating frequency.

1. INTRODUCTION

Radio frequency identification (RFID) is a wireless communication technology used to uniquely identify tagged objects or people. RFID is used for automatic identification with many advantages over the past automatic identification systems such as independence of line-of-sight operation or direct contact with the reader. The RFID system consists of three parts: a reader, a host, and a tag. A reader antenna communicates with the tag antenna with an attached microchip that stores object data [1, 2]. Thus, the RFID tag and reader antenna play the major role in RFID system operation. The RFID reader

Received 19 December 2011, Accepted 2 February 2012, Scheduled 15 February 2012

* Corresponding author: Hend Abd El-Azem Malhat (er_honida@yahoo.com).

antenna is designed with circularly polarized (CP) operation because the tag antenna (which is linearly polarized) will receive enough power from the transmitter irrespective of its orientation. A CP antenna with a relatively low profile, small size, lightweight, high gain, and high front-to-back ratio is required in a portable RFID reader [3, 4]. An antenna with higher gain helps to increase the read range of the reader for the same transmitted RF power. Fixed-reader antennas are becoming more complex microstrip patch arrays with high gain, a relatively narrow beam and low side lobe level [5, 6]. Problems that may arise with conventional RFID readers include: 1) the reader may detect tags that are not in the reader coverage area, 2) the tags may be located adjacent to the reader antenna thus blocking its field, and in some applications, tags may be located in the near-field region of the reader antenna and not in its far-field region as is usually the case in standard communication systems [7].

Recently, a reader phased array antenna exhibiting a near-field (NF) focused radiation, which is able to maximize the field amplitude in a size-limited spot within the antenna near-field region, while not affecting the field strength far from the antenna (far-field region) is introduced [7]. NF-focusing radiation is used in RFID reader to increase the field incident on the tags at allowed effective isotropic radiated power. Phased array antennas suffer from complicated beam-forming networks, complex feeding circuit and relatively high power loss. Phased array problems are overcome using reflectarray introduced in [7, 8]. Some of the phased array limitations have been overcome using reflectarray in [9, 10] for RFID reader. The advantages of reflectarray are easy to fabricate, low profile and has no insertion loss. But, the reflectarray requires an offset feed to avoid blockage losses. This offset feed increases the angle of incidence to the individual elements, thus reducing the reflectarray gain and complicating the design [11, 12]. Transmitarray is similar to the reflectarray, but the incident wave is not reflected, but passes through the antenna structure as it is collimated into a plane wave [13, 14]. Thus the feed horn is positioned directly in front of the array, cannot interfere with the transmitted and received waves, and there is no blockage loss. Dielectric resonator antennas (DRA) have many applications in wireless communication systems over a wide frequency range from 1.3–40 GHz. DRAs offer many advantages such as low profile, low cost, ease of excitation and high radiation efficiency [15]. The DRA have been applied in RFID applications at 5.8 GHz for portable reader [3] and fixed reader [7]. The DRA offer wide bandwidth with reduced size compared with conventional printed antennas.

In this paper, Transmitarray using square DRA is introduced

for fixed RFID reader antenna. The NF-focused transmitarray is introduced for RFID applications and compared with the far-field transmitarray RFID reader. The array is modeled and designed using the finite integral technique (FIT) [16] and the results are compared with those calculated by the transmission line model (TLM) [17] for verification. The two methods selected are based on different principles and are most suitable for the complex array structure.

2. NUMERICAL RESULTS

Considering the array placed in x-y plane illuminated by a horn antenna. As shown in Fig. 1, the phase compensation is accomplished by varying the phase of each element (φ_i) according to the square DRA element position in the array (x_i, y_i), the feed location (x_f, y_f), and the output beam direction (θ_o, φ_o) as follows:

$$\begin{aligned} \varphi_i(x_i, y_i) &= k_o(d_i - \sin\theta_o(x_i\cos\varphi_o + y_i\sin\varphi_o)) \\ d_i &= \sqrt{(x_i - x_f)^2 + (y_i - y_f)^2 + z_f^2} \end{aligned} \tag{1}$$

where k_o is the propagation constant, and d_i is the distance from the feed horn to the ith element.

In this paper, the desired phase shift is obtained by changing the side length of each square DRA element to change its size. The unit cell in the transmitarray consists of three-layered structure separated by air gap $S = 5.5$ mm between the layers. Each layer consists of square DRA with dielectric constant $\varepsilon_{\mathrm{rd}} = 10.9$, height $h = 5$ mm, and variable square cross-section side length L which is used to adjust the phase

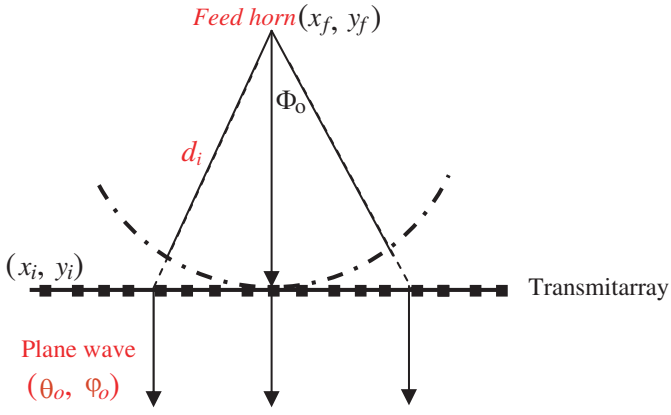

Figure 1. The array structure for the phase compensation.

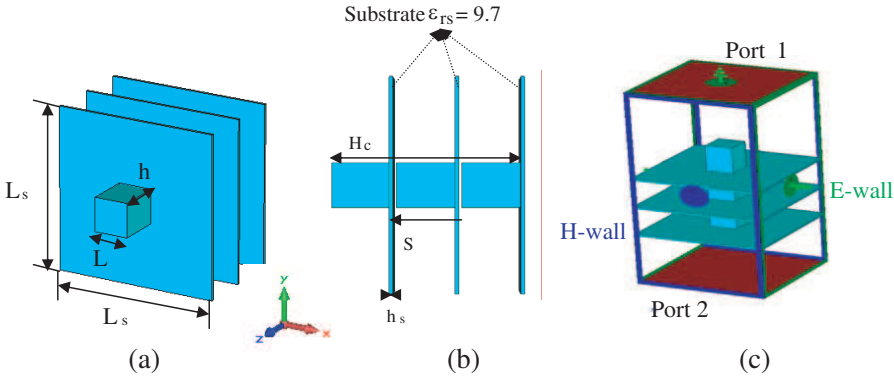

Figure 2. The geometry of the multilayer unit cell and the waveguide simulator with appropriate E and H boundary conditions to support Infinite periodic array. (a) 3-D view. (b) Side view. (c) Wave guide simulator.

of each element. The square DRA is mounted on dielectric substrate with dielectric constant $\varepsilon_{\mathrm{rs}} = 9.7$, total size ($L_s \times L_s = 24 \times 24\,\mathrm{mm}^2$), thickness $h_s = 0.381\,\mathrm{mm}$, and total unit cell height H_c of 17.143 mm. The configuration of the proposed unit cell is designed at 5.8 GHz as shown in Fig. 2. A waveguide simulator is used to calculate the compensation phase of each element by simulating an infinite array of identical elements as shown in Fig. 2(c). For a unit cell, in waveguide simulator the mutual coupling between the elements and the surface waves on the substrates are ignored. The limitations of the infinite array approach are: first, all elements on a layer are identical which is not the real case. Second, the transmitarray itself is not infinite in extent. Thus, the edges effect such as diffraction is not taken into account in the simulator. In the design of the transmitarray the dimensions of the unit cell and the number of layers are optimized to give the above requirements for the magnitude and phase of the transmission coefficient, S_{21} [18, 19]. There are two main challenges: first, the magnitude of S_{21} will be approximately equal one, and then no signal will be reflected from the structure. Second, the phase change of S_{21} must have a tunable range of 2π radians such that the value of 350° phase shift can be achieved. The magnitude and phase responses of the transmission coefficient, S_{21} of the unit cell with varying its square DRA cross-section side length L are calculated using FIT and the results are compared with TLM as shown in Fig. 3. Good agreement between the two approaches is obtained. The minimum value of the transmission magnitude experienced by the structure is $-1.5\,\mathrm{dB}$, while

the transmission phase covers approximately 353° degrees in total. Also, it can be seen that for small size cell and up to about 5 mm cross-section side length of the DRA element, the cell is almost transparent to the 5.8 GHz wave but with a small phase shift within the range 0° to −20°. The high value of the magnitude of the transmission coefficient means that the incident plane wave suffers from small reflection by the DRA elements, thus high transmission is obtained.

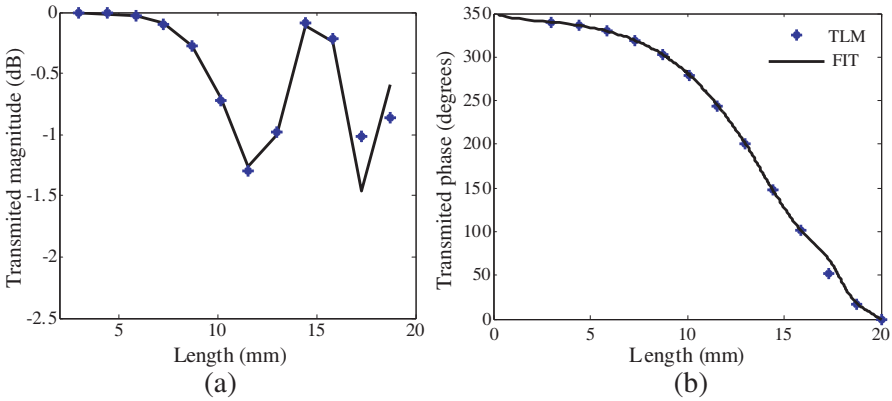

Figure 3. Transmission magnitude and phase versus side-length L of the square DRA element. (a) Transmission magnitude. (b) Transmission phase.

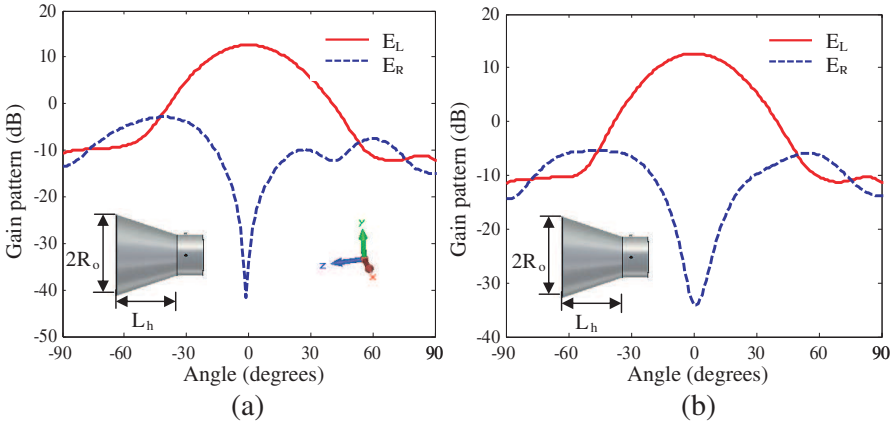

Figure 4. The gain patterns of the circular horn in different planes at 5.8 GHz. (a) H-plane. (b) E-plane.

3. FAR-FIELD FIXED RFID READER TRANSMITARRAY

A circular horn is used to feed the transmitarray with radius $R = 4\,\text{cm}$, and length $L_h = 5\,\text{cm}$ at 5.8 GHz. The left-hand and right-hand polarization radiation patterns of the circular horn in H-plane and E-plane are shown in Fig. 4 at 5.8 GHz. The right-hand polarization (cross-polar) level is lower than $-46\,\text{dB}$ in the broadside direction. Fig. 5 shows the configuration of 9×9 multilayered square DRA transmitarray. The dimensions of each cell in the array is $(L_s \times L_s \times H_c)$,

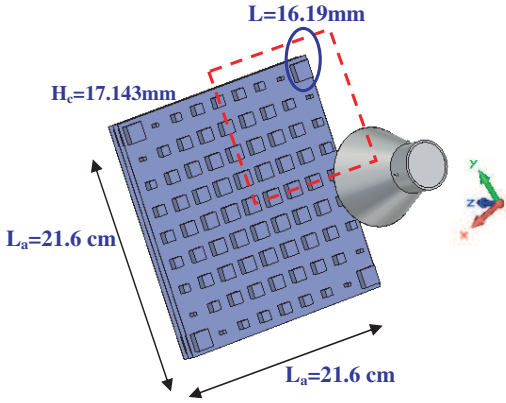

Figure 5. The construction of 9×9 multilayered square DRA transmittarray at 5.8 GHz.

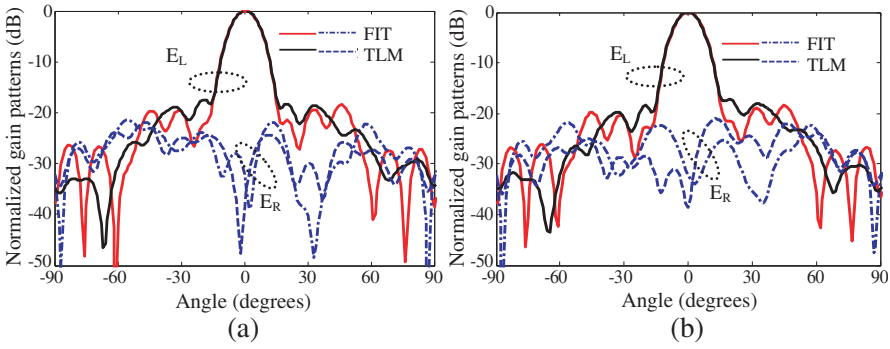

Figure 6. The gain patterns of the of 9×9 multilayered DRA transmittarray at 5.8 GHz in different planes. (a) H-plane. (b) E-plane.

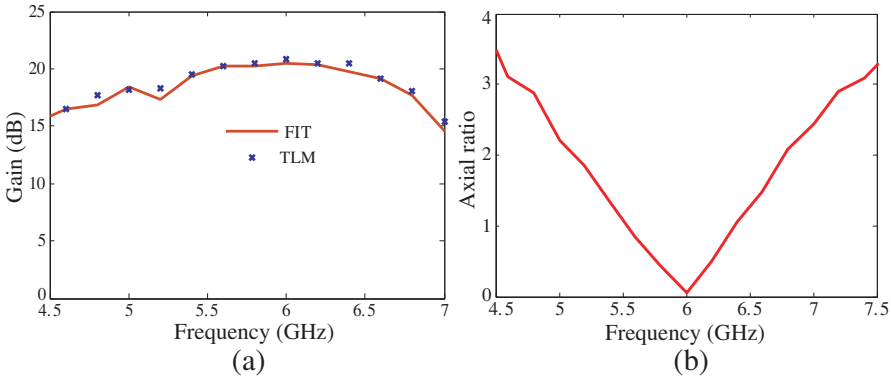

Figure 7. (a) Gain versus frequency of the multilayerd DRA transmitctarray. (b) Axial ratio versus frequency of the multilayerd DRA transmittarray.

with a center to center separation distance of $L_s = 24\,\text{mm}$. It is covering an area of $L_a \times L_a = 21.6 \times 21.6\,\text{cm}^2$. The horn is located at a distance of 28.4 cm from the transmitarray aperture. The transmitarray is symmetrical around the x-axis and y-axis. The compensation phase and the corresponding cross-section DRA side length L of each cell in the first quadrant of the transmitarray are presented in Table 1. The left-hand and right-hand radiation polarization patterns for the transmitarray in different planes at 5.8 GHz are shown in Fig. 6. The field computation are based on full-wave analysis of the problem and is take into consideration the effect of the mutual coupling between the elements and the surface waves on the substrates. The right-hand polarization level is lower than $-31\,\text{dB}$ in the H-plane axial direction at the designed frequency. The dominance of the left-hand polarization (co-polarized) field fails at $\theta = \pm 20^\circ$. The side lobe levels (SLL) in the H- and E-planes are approximately $-22\,\text{dB}$ and $-21.5\,\text{dB}$, respectively. This difference is likely due to the asymmetry in the circular horn feed resulting in different aperture illuminations in the two planes. The gain of the transmitarray against the frequency is shown in Fig. 7(a). The peak gain is 20.2 dB. The frequency band with the variation of the gain around 1 dB from the peak value (1 dB gain bandwidth) is 1.4 GHz (24.1%). The axial ratio versus frequency is shown in Fig. 7(b). The array produces circular polarization in the axial direction with axial ratio, AR $< 3\,\text{dB}$ and covers a range of 2.8 GHz.

Table 1. The phase shift and DRA-side cross section length (L) relevant to the elements of the first-quadrant array for the non-focused transmitarray.

261.88°	270.63°	296.61°	339.08°	36.88°
9.46 mm	8.97 mm	6.9 mm	3 mm	16.19 mm
199.32°	208.4°	235.35°	279.38°	339.08°
11.74 mm	11.48 mm	10.59 mm	8.4 mm	3 mm
153.13°	162.48°	190.19°	235.35°	296.61°
12.88 mm	12.66 mm	11.98 mm	10.59 mm	6.9 mm
124.77°	134.28°	162.48°	208.4°	270.63°
13.56 mm	13.33 mm	12.66 mm	11.48 mm	8.97 mm
115.2°	124.77°	153.13°	199.32°	261.88°
13.77 mm	13.56 mm	12.88 mm	11.74 mm	9.46 mm

4. NEAR-FIELD FOCUSED FIXED RFID READER TRANSMITARRAY

The NF-focused array is achieved by adding proper phase shift to each DRA element in the transmitarray in order to maximize the radiated field in a limited sized spot in the near field region at a distance $z = R_o$ from the transmitarray aperture. For the NF-focused transmitarray, the phase shift of the ith element can be calculated from,

$$\phi_{iNF} = \frac{2\pi}{\lambda}\left(\sqrt{x_i^2 + y_i^2 + R_o^2} - R_o\right) \tag{2}$$

The real part of the Poynting vector is the active power density while the magnitude of its imaginary part is the reactive power density [20]. Adding the above phase shift to Equation (1), the transmitarray elements results in focusing both the active and reactive power density at the focal plane. The ratio between the active power density and the reactive power density is very large in this case. This is due to the fact that the focal plane is very close to the near edge of the Fresnel region. Thus, only the active radiated power density will be taken into account and is given by

$$S = \left\|\mathrm{Re}\left(\vec{S}\right)\right\| = \left\|\mathrm{Re}\left(\vec{E} \times \vec{H}^*\right)\right\| \tag{3}$$

The equivalent plane wave power density p is defined from the

E-field or the H-field as follows [20]

$$p = S_e = \frac{\left\|\vec{E}_x\right\|^2 + \left\|\vec{E}_y\right\|^2 + \left\|\vec{E}_z\right\|^2}{\eta_o},$$
$$\text{or} \qquad p = S_h = \eta_o \left(\left\|\vec{H}_x\right\|^2 + \left\|\vec{H}_y\right\|^2 + \left\|\vec{H}_z\right\|^2\right) \tag{4}$$

where $\eta_o = 377\,\Omega$. The 3-dB beamwidth in the focal plane is defined as the transmitarray spot size. The spot area radius W of a NF-focused planar transmitarray is given by [21]

$$W = 0.8868\ R_o \cdot \frac{\lambda}{L_a} \tag{5}$$

where L_a is the total transmitarray length, $L_a = 21.6\,\text{cm}$, $R_o = 40\,\text{cm}$, and $\lambda_o = 5.17\,\text{cm}$. The geometry of the 9×9 NF-focused transmitarray with its focus is at distance $z = R_o$ from the transmitarray aperture is shown in Fig. 8. The compensation phase and the corresponding DRA cross-section side length of each cell in the first quadrant of the tansmitarray are shown in Table 2. The phase variation extends from 0 to 150° degrees. The distribution of the normalized power density for the non-focused transmitarray ($\varphi_{\text{iNF}} = 0$) and the NF-focused transmitarray on the array aperture in x-y plane at $z = R_o = 40\,\text{cm}$ (i.e., at the focal plane) are shown in Fig. 9.

The power density decays slowly for the non-focused transmitarray, while there is a fast decay for the NF-focused transmitarray from the maximum value at the transmitarray axis. Contour plot of the normalized power density in the focal x-y plane for the non-focused

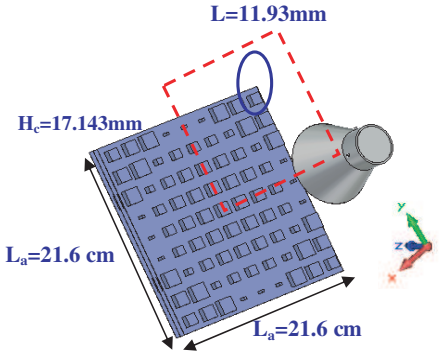

Figure 8. The construction of 9×9 NF-focused multilayered DRA transmittarray at 5.8 GHz.

Table 2. The phase shift and DRA-side cross section length (L) relevant to the elements of the first-quadrant array for the NF-focused transmitarray.

340.93° 3 mm	354.55° 3 mm	35.1° 16.22 mm	101.66° 14.12 mm	192.87° 11.93 mm
244.06° 10.24 mm	258.07° 9.61 mm	299.75° 6.53 mm	8.12° 17.04 mm	101.66° 14.12 mm
173.11° 12.4 mm	187.425° 12.06 mm	229.75° 10.8 mm	299.75° 6.53 mm	35.1° 16.22 mm
129.77° 13.45 mm	144.28° 13.1 mm	187.42° 12.06 mm	258.07° 9.61 mm	354.55° 3 mm
115.2° 13.77 mm	129.772° 13.45 mm	173.11° 12.4 mm	244.06° 10.24 mm	340.93° 3 mm

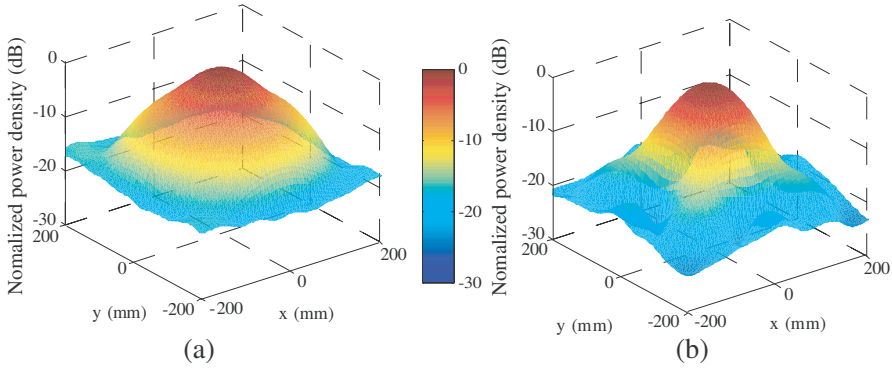

Figure 9. A 3-D plot of the simulated normalized power density of the 9×9 multilayered DRA transmitarray for both the non-focused and NF-focused transmitarray. (a) Non-focused transmitarray ($\varphi_i = 0$). (b) NF-focused transmitarray.

transmitarray and the NF-focused transmitarray are shown in Fig. 10. It is clear that the contours are closer to each other for the NF-focused compared to the separation between the contours for the uniform phase case. The radius of the 3-dB spot area of the NF-focused transmitarray aperture is 7.84 cm at the focal plane. The −10 dB contour curve for the NF-focused transmitarray is 90.5 mm while for the non-focused transmitarray is 152.5 mm. Fig. 11 gives the variation of the simulated normalized power density patterns along the x-axis and y-axis

for both transmitarrays at the focal plane. The SLL is −17.6 dB for the NF-focused transmitarray. The position of the first side lobe of the NF-array is actually situated in the main beam of the non-focused transmitarray. The distribution of the radiated field axial ratio at the focal plane of the transmitarrays is depicted in Fig. 12. The proposed NF-focused array gives circularly polarized fields in the region around the focus in a wider area relative to that for the uniformly phased array. Nearly the same 3-dB axial ratio contour curve is obtained for both the transmitarrays with average radius of 90 mm.

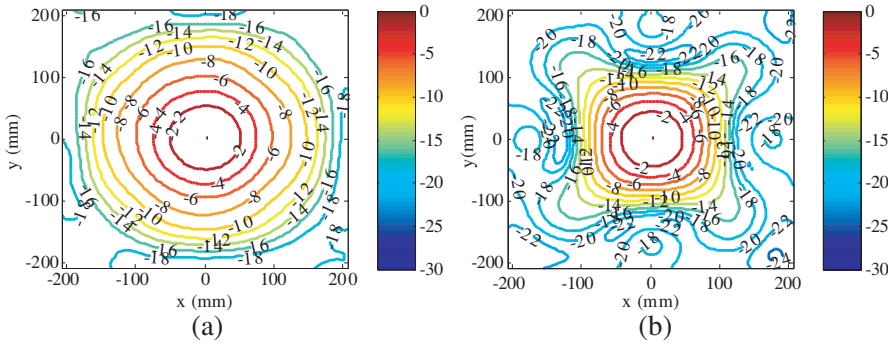

Figure 10. A contour plot of the simulated normalized power density of the 9 × 9 multylayered DRA transmitarray in the transverse plane for both the non-focused and NF-focused transmitarray at $z = R_o =$ 40 cm. (a) Non-focused transmitarray. (b) NF-focused transmitarray.

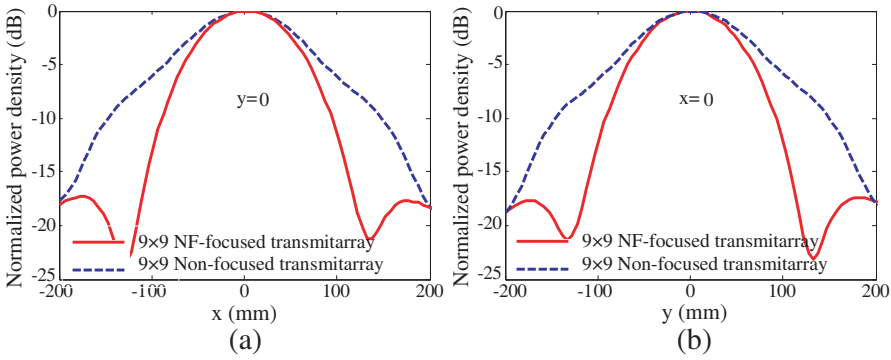

Figure 11. Simulated normalized power density along the transverse direction at $z = R_o =$ 40 cm from the antenna aperture. (a) x-axis. (b) y-axis.

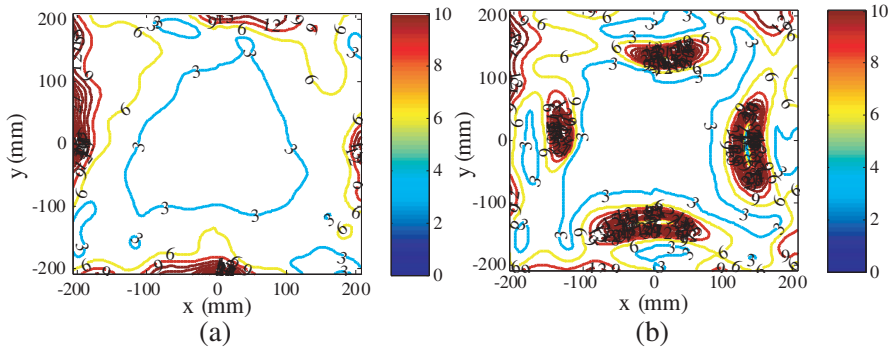

Figure 12. A contour plot of the simulated axial ratio of the 9×9 multilayered DRA transmitarray in the transverse plane for both the non-focused and NF-focused array at $z = R_o = 40\,\text{cm}$. (a) Non-focused transmitarray. (b) NF-focused transmitarray.

5. CONCLUSION

In this paper, a design of 9×9 square DRA transmitarray at 5.8 GHz for far-field RFID applications is introduced. The unit cell consists of three layered square DRA element mounted on dielectric substrate. The dimensions of the DRA are optimized using the finite integral technique for the phase distribution of the transmission coefficient. The transmission line method is used to validate the results. The transmitarray introduces a left-hand circular polarization with right-hand circular polarization (cross-polar) level lower than $-31\,\text{dB}$ at the designed frequency with SLL of $-22\,\text{dB}$. The maximum gain is 20.2 dB with 1 dB gain bandwidth of 1.4 GHz for the far-field transmitarray. A design of 9×9 near-field focused DRA transmitarray for fixed RFID reader antenna at 5.8 GHz is investigated. The properties of the NF-focused transmitarray are compared with the far field transmitarray designed at the same operating frequency. The 3-dB spot area radius of the NF-focused transmitarray aperture is 7.84 cm at the focal plane $z = R_o = 40\,\text{cm}$ with SLL of $-17.6\,\text{dB}$. The position of the first side lobe of the NF-array is actually situated in the main beam of the non-focused transmitarray. The transmitarray produces circular polarization, AR $< 3\,\text{dB}$, over the array aperture at the focal plane at $z = R_o = 40\,\text{cm}$. nearly the same 3-dB axial ratio contour curve is obtained for both the transmitarrays with average radius of 90 mm.

REFERENCES

1. Finkenzeller, K., *RFID Handbook: Radio-frequency Identification Fundamentals and Applications*, 2nd Edition, Wiley & Sons, Inc., New Jersey, USA, 2004.
2. Manish, B. and M. Shahram, *RFID Field Guide: Deploying Radio Frequency Identification Systems*, Prentice Hall PTR, 2005.
3. Zainud-Deen, S. H., H. A. Malhat, and K. H. Awadalla, "Circular polarized dielectric resonator antenna for portable RFID reader using a single feed," *International Journal of Radio Frequency Identification & Wireless Sensor Networks*, Vol. 1, No. 1, 2011.
4. Zainud-Deen, S. H., H. A. Malhat, and K. H. Awadalla, "Octafilar helical antenna for handheld UHF-RFID reader," *International Journal of Radio Frequency Identification & Wireless Sensor Networks*, Vol. 1, No. 1, 2011.
5. Liao, W. J., S. H. Chang, Y. C. Chu, and W. S. Jhong, "A beam scanning phase array for UHF RFID readers with circularly polarized patches," *Journal of Electromagnetic Waves and Applications*, Vol. 24, Nos. 17–18, 2383–2395, 2010.
6. Fan, Z., S. Qiao, J. T. Huang-Fu, and L.-X. Ran, "A miniaturized printed dipole antenna with V-shaped ground for 2.45 GHz RFID readers," *Progress In Electromagnetics Research*, Vol. 71, 149–158, 2007.
7. Zainud-Deen, S. H., H. A. Malhat, and K. H. Awadalla, "Near-field focused DRA array for fixed RFID reader," *International Journal of Radio Frequency Identification & Wireless Sensor Networks*, Vol. 1, No. 1, 2011.
8. Chou, H. T., T. M. Hung, N. N. Wang, H. H. Chou, C. Tung, and P. Nepa, "Design of a near field focused reflectarray antenna for 2.4 GHz RFID reader applications," *IEEE Trans. Antennas Propag.*, Vol. 59, No. 3, 1013–1018, March 2011.
9. Chou, H. T., P. Hsueh, T. Hung, L. Kuo, and Y. Ze, "Near-zone focused radiations of reflectarray antennas for RFID applications at 0.9 and 2.4 GHz," *Proc. IEEE Antennas and Propagation Soc. Int. Symp.*, Vol. 1, 1727–1730, USA, June 2011.
10. Chou, H. T., P. Hsueh, T. Hung, L. Kuo, and Y. Ze, "Numerical synthesis of reflectarray antenna for optimum near-field radiation at 2.4 GHz," *Proc. IEEE Antennas and Propagation Soc. Int. Symp.*, Vol. 1, 1731–1734, USA, June 2011.
11. Huang, J. and J. A. Encinar, *Reflectarray Antennas*, John Wiley & Sons, Inc., Hoboken, NJ, 2007.

12. Zaiund-Deen, S. H., S. M. Gaber, A. M. Abd-Elhady, A. A. Kishk, and K. H. Awadalla, "Wideband perforated rectangular dielectric resonator antenna reflectarray," *Proc. IEEE Antennas and Propagation Soc. Int. Symp.*, Vol. 1, 113–116, USA, June 2011.
13. Ryan, C. G. M., M. R. Chaharmir, J. Shaker, J. R. Bray, Y. M. M. Antar, and A. Ittipiboon, "A wideband transmitarray using dual-resonant double square rings," *IEEE Trans. Antennas Propag.*, Vol. 58, No. 5, 1486–1493, May 2010.
14. Lau, J. Y. and S. V. Hum, "Analysis and characterization of a multipole recon?gurable transmitarray element," *IEEE Trans. Antennas Propag.*, Vol. 59, No. 1, January 2011.
15. Petosa, A., *Dielectric Resonator Antenna Handbook*, Artech House Inc., Norwood, 2007.
16. Schuhmann, R., T. Weiland, W. H. Schilders, E. J. Maten, and S. H. Houben, "Recent advances in finite integration technique for high frequency applications," *Scientific Computing in Electrical Engineering*, Vol. 4, 46–57, 2004.
17. Christopoulos, C., *The Transmission Line Modeling Method (TLM)*, The Institute of Electrical and Electronics Engineers, Inc., 1995.
18. Lam, K., S. Kwok, Y. Hwang, and T. K. Lo, "Implementation of transmitarray antenna microstrip patches concept by using aperture-coupled," *Asia Pacific Microwave Conference*, 433–436, 1997.
19. Mcgrath, D. T., "Planar three dimensional constrained lenses," *IEEE Trans. Antennas Propag.*, Vol. 34, No. 1, 46–50, January 1986.
20. Adanel, Y., M. Wongl, C. Dale', and J. Wiartl, "Near field power density characterization of radio base station antennas using spherical harmonics optimization techniques," *European Conference on Wireless Technology*, 121–124, Amsterdam, Holland, 2004.
21. Hansen, R. C., "Focal region characteristics of focused array antennas," *IEEE Trans. Antennas Propag.*, Vol. 33, No. 12, 1328–1337, December 1985.